energies

MDPI

Article

Energy and Exergy Analyses of Geothermal Organic Rankine Cycles Considering the Effect of Brine Reinjection Temperature

Yuan Zhao [1], Chenghao Gao [1], Chengjun Li [1], Jie Sun [2,3], Chunyan Wang [2], Qiang Liu [2,*] and Jun Zhao [4]

[1] Powerchina Huadong Engineering Corporation Limited, Hangzhou 311122, China
[2] State Key Laboratory of Petroleum Resources and Prospecting, College of Mechanical and Transportation Engineering, China University of Petroleum, Beijing 102249, China
[3] Patent Examination Cooperation (Jiangsu) Center of The Patent Office, China National Intellectual Property Administration, Suzhou 215163, China
[4] Key Laboratory of Efficient Utilization of Low and Medium Grade Energy, Ministry of Education, Tianjin University, Tianjin 300350, China
* Correspondence: qliu@cup.edu.cn

Abstract: The organic Rankine cycles (ORCs) have been used to convert low-enthalpy geothermal brine into power. Parameter optimization and working fluid selection are the main approaches to enhance geothermal ORC performance. This work uses environmentally friendly fluids, including R1224yd(Z), R1233zd(E), R1336mzz(Z), R601 and R601a, as the geothermal ORC working fluids. The evaporation temperatures of the selected fluids were optimized to maximize the cycle net power outputs. The thermodynamic characteristics are investigated with the consideration of the influence of the allowed reinjection temperature (ARIT). Among the selected fluids, R1224yd(Z) has the highest optimal evaporation temperature with the maximum turbine power output for a brine inlet temperature (BIT) higher than 120 °C, especially at a lower allowed reinjection temperature. However, the parasitic power consumption by the pumps in an ORC with R1224yd(Z) is also higher than with the other four fluids. The net power output for ORC with R1336mzz(Z) is slightly more than that with R1224yd(Z). Although the optimal evaporation temperature for a RORC is lower than that for an ORC, the higher preheater inlet temperature leads to a higher geothermal heating exergy efficiency and more power output for a BIT less than 120 °C. The RORC with R1336mzz(Z) produces 2.6% more net power than an ORC for a brine inlet temperature of 100 °C. As the ARIT increases from 70 °C to 75 °C, the plant exergy efficiencies of ORCs are decreased by 6–8% for a geothermal brine inlet temperature of 100 °C.

Keywords: geothermal power generation; organic Rankine cycle; exergy analysis; working fluid; optimization

Citation: Zhao, Y.; Gao, C.; Li, C.; Sun, J.; Wang, C.; Liu, Q.; Zhao, J. Energy and Exergy Analyses of Geothermal Organic Rankine Cycles Considering the Effect of Brine Reinjection Temperature. *Energies* **2022**, *15*, 6230. https://doi.org/10.3390/en15176230

Academic Editor: Kyung Chun Kim

Received: 11 August 2022
Accepted: 24 August 2022
Published: 26 August 2022

1. Introduction

The utilization of renewable energy for power generation is an efficient approach to reduce greenhouse gas emissions and fossil fuel consumption. The geothermal energy has the distinctive characteristics of being stable, being independent of weather conditions and having huge storage capability [1,2]. Geothermal power plants can stabilize power generation and reduce the impact on power grid stability, compared to solar and wind power plants. The worldwide geothermal power capacity had reached 15.85 GW in 2021 [3], while the installed capacity of geothermal power plants in China is only 43 MW so far [1]. The organic Rankine cycles (ORCs) are widely used to convert low-enthalpy geothermal water into electricity owing to its stability, flexibility and safety [4–6].

The thermodynamic perfectness of a basic ORC with a single pressure evaporation is relatively low due to the greater irreversible losses mainly caused by the large temperature difference between the working fluid and the brine. The exergy losses during the working fluid preheating and isothermal evaporating are the greatest, which exceed 30% of the total

exergy losses [7,8]. Thus, improving the matches between the working fluid and the brine temperatures is a crucial issue for reducing the exergy losses during evaporation [7,9]. The cycle configuration improvement [10–13], parametric optimization [14–16] and working fluid selection [17,18] are the main approaches to improve the ORC thermodynamic characteristics. Li et al. [19] analyzed the thermodynamics of dual- and single-pressure ORCs with nine selected working fluids for heat sources ranging from 100 to 200 °C without a limit on the outlet temperature. Their results showed that the net power outputs were boosted by 21.4–26.7% by dual-pressure evaporation. Finally, they proposed a criterion to design the optimal cycle for various heat source temperatures. Li et al. [20] also investigated the thermo-economics of dual-pressure evaporation ORCs with separate and induction turbine layouts. Luo et al. [21] proposed a multi-pressure evaporation ORC with liquid separation condensation using zeotropic mixtures. They pointed out that the multi-pressure ORC produced 13.1–26.2% more net power than a simple ORC. Karimi and Mansouri [22] investigated the thermodynamic and economic characteristics of basic ORCs, regenerative ORCs and two-stage evaporation ORCs. They found that the dual-pressure ORCs and regenerative ORCs produced more electricity than the basic ORCs. Du et al. [23] studied the off-design performance of a dual-pressure ORC and a basic ORC using R245fa. Their results showed that the dual-pressure ORC generated 18.39% more net power than a basic ORC. They found that the net power difference between the dual-pressure ORC and the basic ORC increased with increasing hot water mass flow rate and inlet temperature. Bina et al. [24] analyzed the thermo-economic performance of a basic ORC, a dual fluid ORC, a regenerative ORC and an ORC with an internal heat exchanger (IHE) driven by the geothermal water at 165 °C from a flash cycle. They demonstrated that the ORC with an IHE was the best choice. Yari [25] determined the optimum design parameters and compared the thermodynamic performance of different binary power plants at a geothermal fluid temperature of 180 °C. Therefore, their results showed that the ORC with an IHE (also referred to as a recuperator) was a promising option.

Selecting the superior working fluid is a main measure to enhance the thermodynamics of geothermal ORCs. Generally, to select the proper fluid for an ORC shall consider three aspects, the cycle layout, the geothermal source conditions, and the operating constraints on the ORC. The flammability, toxicity, thermal stability, cost and potential hazards of the organic fluid to the environment also influence the working fluid selection [26,27]. Working fluids used for geothermal ORCs should have a low boiling point to ensure that the condensation pressure is greater than the ambient pressure. The organic fluids, such as CFCs (chlorofluorocarbons), HCFCs (hydrochlorofluorocarbons), HFCs (hydrofluorocarbons) and HCs (hydrocarbons), with the critical temperature in the range of 100–200 °C were selected as the working fluids for geothermal ORCs. However, the CFCs and HCFCs have been banned because of their higher ODPs (ozone depletion potentials). Traditional HFCs, such as R134a and R245fa, have been widely used in commercial ORCs; however, they are progressively being phased out because of their greater GWPs (global warming potentials) [26]. The most recent HFOs (hydrofluoroolefins), including R1233zd(E) (trans-1-chloro-3,3,3-trifluoropropene), R1224yd(Z) (cis-1-chloro-2,3,3,3-tetrafluoropropene) and R1336mzz(Z) (trans-1,1,1,4,4,4-Hexafluoro-2-butene), have been proved to be alternative working fluids for ORCs [28–33] with smaller environmental risks.

Eyerer et al. [28] experimentally studied the applicability of R1233zd(E) and R1224yd(Z) as alternative fluids to R245fa for ORCs. They found that R245fa generated 9% more power than R1233zd(E) but R245fa was almost 2% less thermally efficient. They pointed out that R1233zd(E) and R1224yd(Z) were suitable drop-in replacements for R245fa, concerning the GWP, thermodynamics and material compatibility. Welzl et al. [29] investigated the isentropic efficiencies of R1336mzz(Z) and R245fa in a scroll expander. Their experimental results showed that the isentropic efficiencies with R1336mzz(Z) were slightly lower than that with R245fa. Dawo et al. [30] experimentally studied the thermodynamics of R1224yd(Z), R1233zd(E), R1336mzz(Z) and R245fa on an ORC test system. They pointed out that R1224yd(Z) and R1233zd(E) were appropriate alternatives for R245fa with similar

expander isentropic efficiencies. Longo et al. [31] studied the thermodynamic and heat transfer characteristics of ORCs and heat pumps using R600a, R1234ze(Z) and R1233zd(E). They found that the efficiency of an ORC using R1233zd(E) was greater than that using R245fa. Qiu et al. [32] experimentally studied the thermodynamics of a micro-CHP system with an ORC using R1223zd(E) and pentane as the working fluids. They demonstrated that the efficiency and electricity output with R1223zd(E) were slightly greater than that with pentane. Ye et al. [33] theoretically and experimentally studied the thermo-economic and environmental performance of ORCs using R12333zd(E), R1234ze(Z), R1366mzz(E) and R245fa for waste heat recovery. They demonstrated that R1233zd(E) has the best thermodynamic performance, followed by R1234ze(Z) and R1366mzz(E).

There are many studies aimed at the thermodynamic performance improvements by adding a recuperator to utilize the waste heat from the turbine exhaust vapor for preheating. However, the recuperator may increase the reinjection temperature, resulting in a decrease in the geothermal energy (exergy) utilization efficiency. Moreover, the reinjection temperature should be high enough to limit the scaling and fouling problems in the heat exchangers and pipes [2,6,14]. The allowed reinjection temperature directly affects the geothermal brine temperature profiles and the ORC thermodynamics [14,34]. However, the influence of the reinjection temperature limit is not much considered in the literature. Therefore, this work focuses on the thermodynamics of geothermal ORCs using low-GWP working fluids, including R1224yd(Z), R1336mzz(Z), R1233zd(E), R600 and R601a, and taking into account the influences of the allowed reinjection temperature and the use of a recuperator. The evaporation temperatures of the selected fluids are optimized to maximize the cycle net power output for various geothermal brine inlet temperatures from 100 to 150 °C and allowed reinjection temperatures from 65 to 75 °C, depending on the geothermal sources and brine characteristics. The geothermal exergy utilization efficiencies at the optimal conditions are analyzed with consideration of the influences of the recuperator and reinjection temperature. Both the cycle internal exergy efficiency and the plant exergy efficiency are discussed to evaluate the ORC thermodynamic perfectness. The thermodynamic characteristics at the optimal conditions of various brine conditions are also compared to find the superior working fluid.

2. Method

2.1. System Description

Thermodynamic characteristics of organic Rankine cycles (ORCs) using dry working fluids are analyzed in this work. The waste heat of the superheated turbine exhaust vapor can be utilized for fluid preheating by a recuperator. Since the temperature difference between the working fluid and the geothermal brine is reduced, the recuperator reduces the exergy losses during the working fluid heat absorption and improves the cycle efficiency; meanwhile, the reinjection temperature can also be increased. Thus, thermodynamic characteristics of ORCs using a recuperator (RORCs) are also studied. The schematics for an ORC and a RORC are shown in Figure 1 with the corresponding *T-s* diagrams shown in Figure 2.

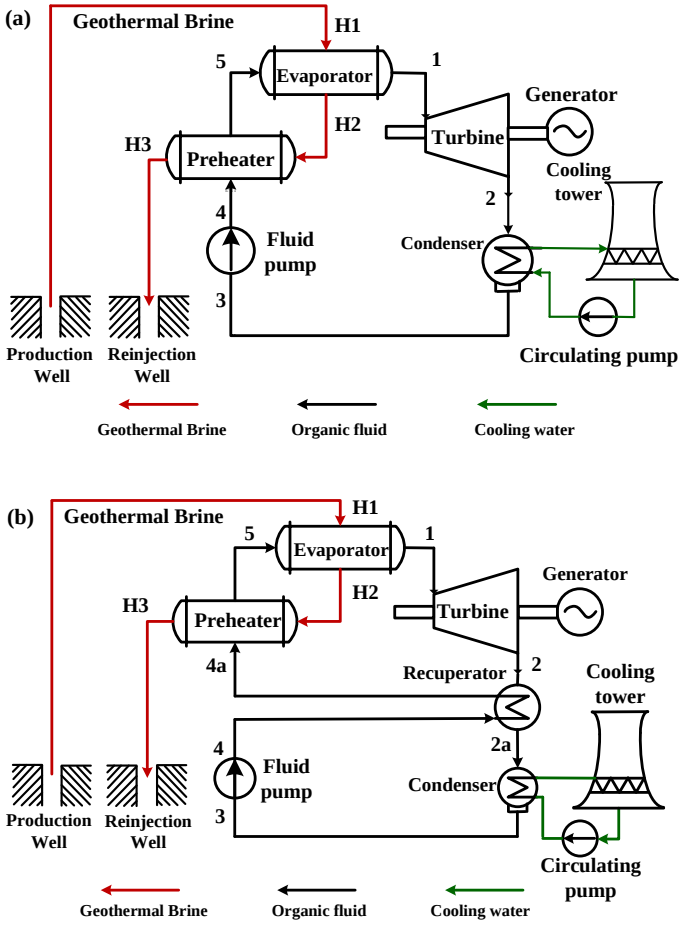

Figure 1. Schematics of (**a**) an ORC and (**b**) RORC with a recuperator.

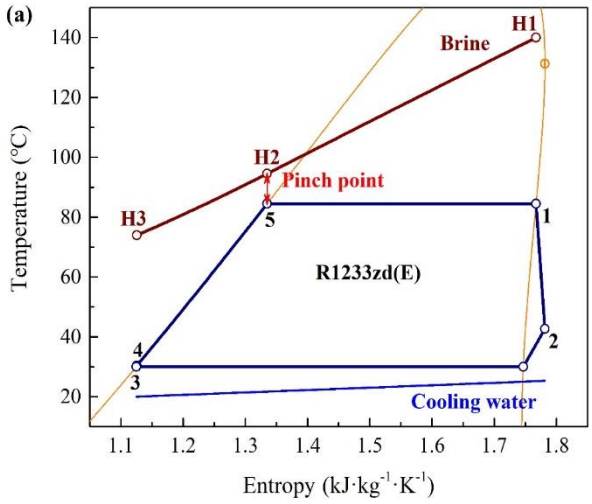

Figure 2. *Cont.*

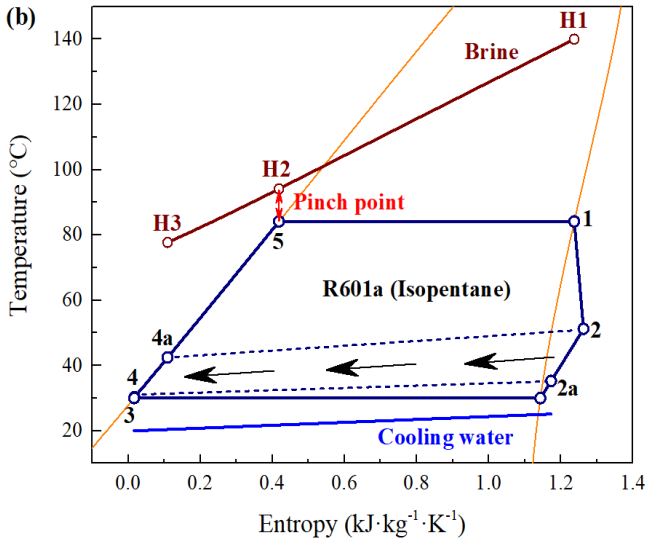

Figure 2. $T-s$ diagram of (**a**) an ORC using R1233zd(E) and (**b**) a RORC using R601a.

2.2. Thermodynamic Model

The mass and energy equations for any steady-state control volumes applied to ORC systems, ignoring the heat losses and the pressure drop, can be expressed as:

$$\Sigma \dot{m}_{\text{in}} = \Sigma \dot{m}_{\text{out}} \tag{1}$$

$$\dot{Q} - \dot{W} = \Sigma \dot{m}_{\text{out}} h_{\text{out}} - \Sigma \dot{m}_{\text{in}} h_{\text{in}} \tag{2}$$

where $\dot{m}$ is the mass flow rate, $\dot{Q}$ is the net heat input, $\dot{W}$ is the net power, h is the specific enthalpy and the subscripts in and out stand for inlet and outlet.

The power generated by the turbine is:

$$\dot{W}_{\text{T}} = \dot{m}_{\text{O}}(h_1 - h_2) = \dot{m}_{\text{O}}(h_1 - h_{2s})\eta_{\text{T}} \tag{3}$$

where the subscript O represents the organic fluid, h_1 and h_2 are the enthalpies at the turbine inlet and outlet and η_{T} is the turbine isentropic efficiency.

The power consumed by the working fluid feed pump for was calculated as:

$$\dot{W}_{\text{FP}} = \dot{m}_{\text{O}}(h_4 - h_3) \tag{4}$$

The power consumed by the circulating pump in the cooling system was calculated as:

$$\dot{W}_{\text{CP}} = \frac{\dot{m}_{\text{CW}} g H}{\eta_{\text{CP}}} \tag{5}$$

where $\dot{m}_{\text{CW}}$ is the cooling water flow rate, g is the gravitational acceleration, H is the circulating pump head and η_{CP} is the circulating pump efficiency.

The net power output by the geothermal ORC system is:

$$\dot{W}_{\text{net}} = \dot{W}_{\text{T}} \eta_{\text{m}} \eta_{\text{g}} - \dot{W}_{\text{FP}} - \dot{W}_{\text{CP}} \tag{6}$$

where η_{m} is the mechanical efficiency and η_{g} is the generator efficiency.

2.3. Exergy Analysis

Exergy balance for any control volume at steady state with negligible potential and kinetic energy changes can be expressed as:

$$\dot{E} - \dot{W} = \Sigma \dot{E}_{\text{out}} - \Sigma \dot{E}_{\text{in}} + \dot{I} \tag{7}$$

where $\dot{E}$ is the exergy and $\dot{I}$ is the exergy destruction.

The geothermal exergy input (total available geothermal exergy) to the ORC system is:

$$\dot{E}_{\text{G,in}} = \dot{m}_{\text{G,in}}[h_{\text{G,in}} - h_0 - T_0(s_{\text{G,in}} - s_0)] \tag{8}$$

where $h_{\text{G,in}}$ and $s_{\text{G,in}}$ are the enthalpy and entropy of the geothermal water at the ORC system inlet, h_0 and s_0 are the reference values of the enthalpy and entropy of the geothermal water at the reference state, the ambient temperature, T_0, was set to be 293.15 K and the ambient pressure was set to be 101.325 kPa (the reference state).

The plant exergy efficiency was defined as:

$$\eta^{\text{ex}}_{\text{plant}} = \frac{\dot{W}_{\text{net}}}{\dot{E}_{\text{G,in}}} \tag{9}$$

The plant exergy efficiency corresponds to the net power output according to Equation (9). The reinjection temperature may be higher than the allowed value for the optimal cycle efficiency for higher brine inlet temperatures (BITs). Therefore, the geothermal exergy utilization efficiency was employed to evaluate the utilization ratio of the geothermal exergy with the selected working fluids for various BITs.

The geothermal exergy utilization efficiency denotes the ratio of the geothermal exergy for heating the working fluid to the total geothermal exergy and can be expressed as:

$$\eta^{\text{ex}}_{\text{GU}} = \frac{\dot{E}_{\text{G,in}} - \dot{E}_{\text{G,out}}}{\dot{E}_{\text{G,in}}} \tag{10}$$

where $\dot{E}_{\text{G,out}}$ is the exergy of the reinjection brine. The geothermal exergy utilization efficiency decreases with increasing reinjection temperature for a given geothermal brine inlet temperature.

The largest irreversible losses in an ORC generally occur in the preheater and evaporator. The exergy analysis employs the geothermal heating exergy efficiency as an indicator to evaluate the exergy utilized by the working fluid from the geothermal brine during the preheating and isothermal evaporating, considering the effects of the allowable reinjection temperature. A higher geothermal heating exergy efficiency means smaller irreversible losses in the preheater and the evaporator. The geothermal heating exergy efficiency was defined as:

$$\eta^{\text{ex}}_{\text{GH}} = \frac{\Delta \dot{E}_{\text{O}}}{\dot{E}_{\text{G,in}} - \dot{E}_{\text{G,out}}} \tag{11}$$

where $\Delta \dot{E}_{\text{O}}$ is the exergy increase of the working fluid (net exergy input to the cycle).

The cycle internal exergy efficiency is employed to evaluate the net power converted from the cycle exergy input. The net power generated by the ORC can be described as the net cycle exergy input subtracting the total exergy losses in the turbine, generator, fluid pump, recuperator, condenser and cooling system. The cycle internal exergy efficiency was defined as:

$$\eta^{\text{ex}}_{\text{cycle}} = \frac{\dot{W}_{\text{net}}}{\Delta \dot{E}_{\text{O}}} \tag{12}$$

Finally, the plant exergy efficiency can also be expressed as:

$$\eta_{\text{plant}}^{\text{ex}} = \eta_{\text{GU}}^{\text{ex}} \eta_{\text{GH}}^{\text{ex}} \eta_{\text{cycle}}^{\text{ex}} \tag{13}$$

2.4. Working Fluid Selection

Only the dry-type fluid was considered in this work. Pentane (R601), isopentane (R601a), trans-1-chloro-3,3,3-trifluoropropene (R1233zd(E)), trans-1,1,1,4,4,4-Hexafluoro-2-butene (R1336mzz(Z)) and cis-1-chloro-2,3,3,3-Tetrafluoropropene (R1224yd(Z)) were selected as the working fluids for the ORCs. R601 and R601a have been widely used as the working fluids for geothermal ORCs, while R1233zd(E), R1224yd(Z) and R1336mzz(Z) are promising alternatives. The five working fluids are environmentally friendly with zero ODP (ozone depletion potential) and smaller GWPs (global warming potential). The properties of the selected working fluids are listed in Table 1 and the saturation curves are plotted on a temperature–entropy diagram, as shown in Figure 3. The thermophysical properties of the working fluids were calculated by REFPROP Version 10.0 [35].

Table 1. Physical and environmental properties of the selected working fluids.

Working Fluid	Tcr (°C)	pcr (MPa)	Safety Class	GWP100yrs
R1224yd(Z)	155.54	3.337	-	1
R1233zd(E)	165.6	3.572	A1	1
R1336mzz(Z)	171.35	2.903	A1	2
R601a	187.2	3.378	A3	~20
R601	196.55	3.368	A3	~20

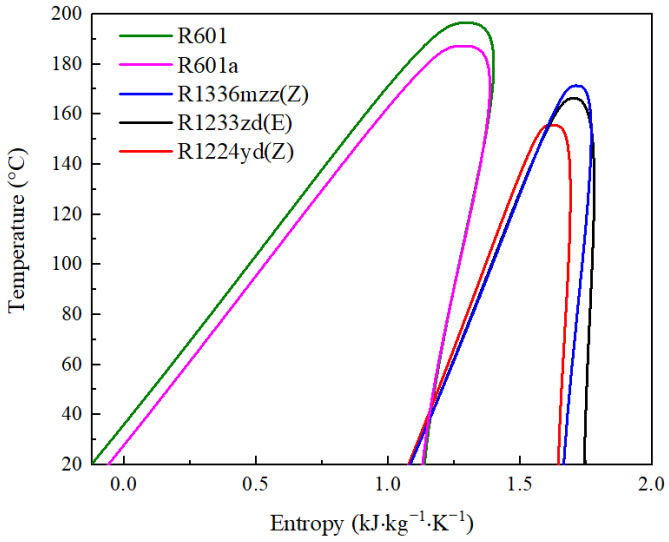

Figure 3. Saturation curves for the selected working fluids on the temperature–entropy diagram.

2.5. Study Cases

The reinjection temperature should keep at a high value to limit silica scaling problems [2,6]. The allowed reinjection temperature varies with the geothermal source characteristics and the reinjection strategy [34,36]. The reinjection temperatures are typically maintained at no less than 65 °C [2], 70 °C [34,37] or 75 °C [34,36], depending on the mineral solubility in the brine. These temperatures were accordingly chosen to investigate the effects of the allowed reinjection temperature on the ORC thermodynamics. The operating parameters and boundary conditions of the ORC systems are listed in Table 2. The saturated ORCs were studied here because the selected working fluids have a high temperature turning point that can avoid two-phase expansion [38]. Therefore, the evaporation

temperatures of the selected working fluids were optimized to maximize the net power output for various brine inlet temperatures and allowed reinjection temperatures.

Table 2. Operating parameters and boundary conditions for the geothermal ORC.

Parameter	Symbol	Value	Unit
Geothermal water flow rate	$\dot{m}_G$	50	kg/s
Geothermal water pressure	p	2	MPa
Evaporator pinch point temperature difference	Δt_E	10	°C
Cooling water inlet temperature	$t_{C,in}$	20	°C
Condenser pinch point temperature difference [39]	Δt_C	5	°C
Condensation temperature	t_C	30	°C
Pinch point temperature difference in the recuperator [40]	Δt_p	5	°C
Turbine isentropic efficiency	η_T	85	%
Turbine mechanical efficiency	η_m	98	%
Generator efficiency	η_g	98	%
Working fluid pump isentropic efficiency [39]	η_{FP}	65	%
Circulating pump head	H	20	m
Circulating pump efficiency	η_{CP}	80	%

3. Results and Discussion

3.1. Optimal Evaporation Temperature

The evaporation temperatures of the selected working fluids were optimized for the maximum net power output. Figure 4 shows the optimal evaporation temperatures of ORCs and RORCs for various brine inlet temperatures (BITs) with allowed reinjection temperatures (ARITs) of 65 °C, 70 °C and 75 °C, respectively. The corresponding reinjection temperatures under the optimal conditions are shown in Figure 5. The optimal evaporation temperature of R1224yd(Z) is the highest, while that of R601 is the lowest for an allowed reinjection temperature of 65 °C, as shown in Figure 4(a1). The optimal evaporation temperature increases by 2.6–3.2 °C for every 5 °C increase in the brine inlet temperature (BIT) with the corresponding reinjection temperatures higher than 65 °C, as shown in Figure 5(a1), when the ARIT is 65 °C. Note that the power generated by the ORC increases over a reinjection temperature range because the increase in the cycle thermal efficiency caused by a higher evaporation temperature is greater than the decrease in the utilized geothermal heat. The reinjection temperature for an ORC using R601 is the highest while that using R1336mzz(Z) is the lowest among the selected five working fluids. The working fluid evaporation temperature increases to better match the temperature profiles during evaporation for a lower BIT as the ARIT increases. When the ARIT increases from 65 °C to 70 °C, the optimal evaporation temperatures increase by 3.8–4.6 °C for a BIT of 100 °C, as shown in Figure 4(a2). Thus, the reinjection temperature is fixed at the allowed value of 70 °C for the maximum heat input, as shown in Figure 5(a2). However, the optimal evaporation temperature does not change with increasing ARIT for a higher BIT. When the BIT is almost higher than 115 °C, the optimal evaporation temperatures of R1233zd(E), R601a and R601 for the ARIT of 70 °C equal to those for the ARIT of 65 °C, as shown in Figure 4a. Similar phenomena are found for R1224yd(Z) and R1336mzz(Z) when the BIT is almost above 120 °C. As the ARIT further increases from 70 °C to 75 °C, the optimal evaporation temperatures of R1224yd(Z) and R1336mzz(Z) increase by 3–4.5 °C for better temperature matches, especially for a lower inlet temperature, as shown in Figure 4(a3). The optimal evaporation temperatures of all the selected fluids increase by around 4.5 °C for a BIT of 100 °C as the ARIT increases from 70 °C to 75 °C, while the optimal evaporation temperatures for R1233zd(E) and R601 only increase within 1 °C for a BIT higher than 140 °C. R1224yd(Z) and R1336mzz(Z) have similar optimal evaporation temperatures, and they are noticeably higher than R601 for an ARIT of 75 °C, as shown in Figure 4(a3), which results in a higher cycle thermal efficiency. For instance, the evaporation temperature of R1224yd(Z) is 5.2 °C higher than that of R601 for a BIT of 150 °C.

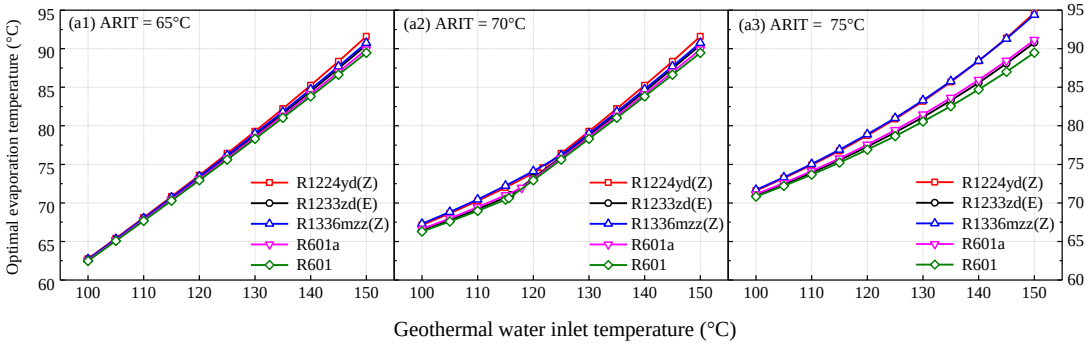

(**a**) ORC

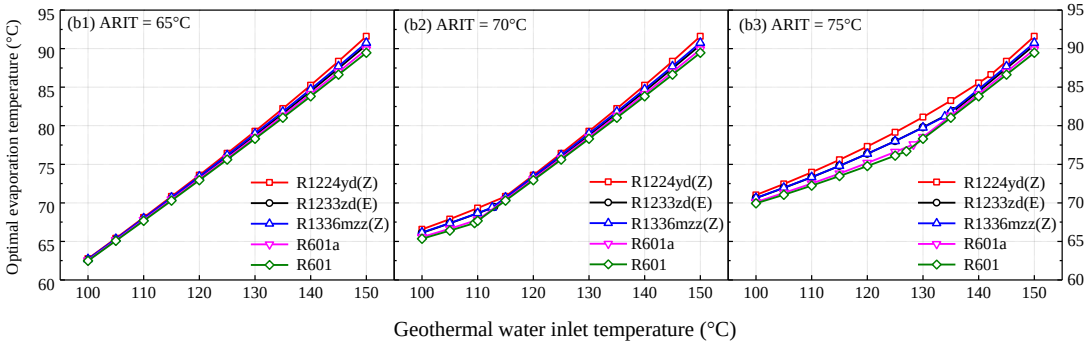

(**b**) RORC

Figure 4. Optimal evaporation temperatures of the selected working fluids for (**a**) ORCs and (**b**) RORCs for various geothermal brine inlet temperatures (BITs) and allowed reinjection temperatures (ARITs).

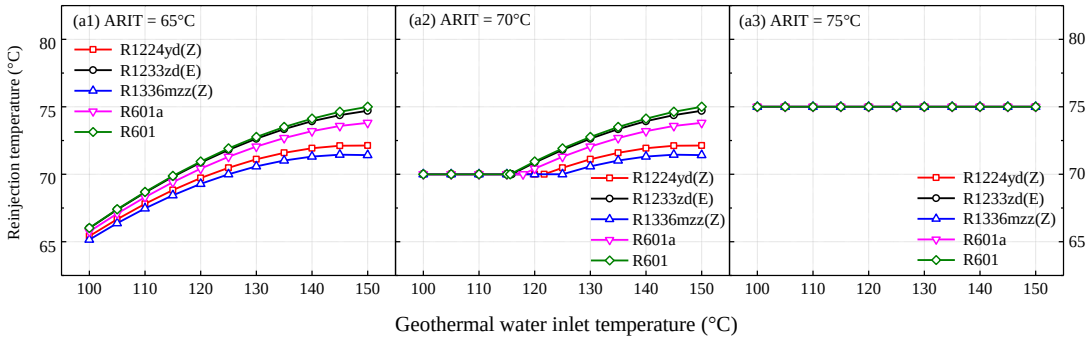

(**a**) ORC

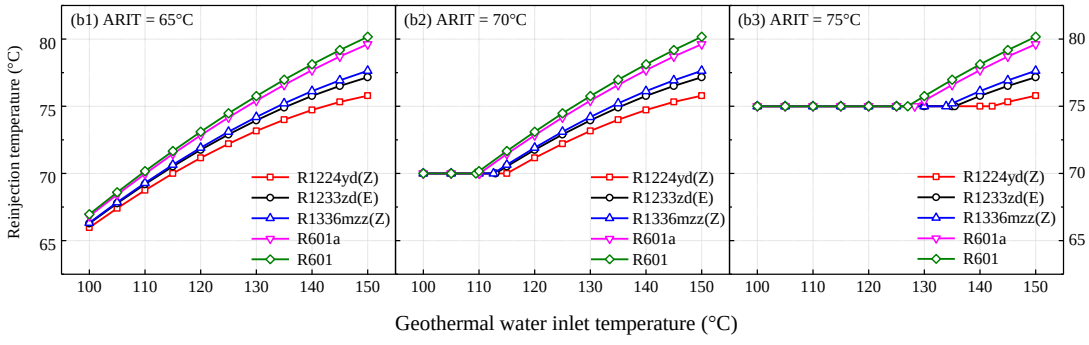

(**b**) RORC

Figure 5. Reinjection temperatures at the optimal conditions for (**a**) ORCs and (**b**) RORCs.

A recuperator recovers part of the waste heat from the turbine exhaust and then increases the preheater inlet temperature that leads to a decrease in cold source losses and an increase in the cycle thermal efficiency. The working fluid temperature increase through the recuperator increases with increasing BIT, since the turbine exhaust temperature also increases. The use of a recuperator does not affect the optimal evaporation temperature for an ARIT of 65 °C, as shown in Figure 4(b1), but the reinjection temperature at the optimal condition of a RORC is higher than that of an ORC, as shown in Figure 5(b1). The turbine exhaust temperature of R1233zd(E) is much lower due to the near-vertical slope of the saturated vapor curve as seen in Figure 3, which leads to a smaller temperature rise in the recuperator; thus, the increase in the reinjection temperature by a recuperator with R1233zd(E) is the lowest among the five working fluids, which ranges from 0.3 °C to 2.5 °C. The temperature increases of R1336mzz(Z), R601a and R601 in the recuperator are 4.9–5.3 °C for a BIT of 100 °C and 13.2–14 °C for a BIT of 150 °C with an ARIT of 65 °C, because of their higher turbine exhaust temperatures. The preheating load for R1336mzz(Z) is higher than R601a and R601 due to the lower latent heat of vaporization for a given evaporation temperature. Therefore, the increase in the reinjection temperature by a RORC with R1336mzz(Z) is slightly higher than that with R601a or R601. RORC increases the reinjection temperature by 1.2–6.2 °C with R1336mzz(Z) and 0.9–5.2 °C with R601. The reinjection temperatures of RORCs using R1336mzz(Z), R601a and R601 are higher than that using R1233zd(E), as shown in Figure 5b.

The optimal evaporation temperature of RORC is lower than that of an ORC due to the pinch temperature difference limit for a BIT less than around 115 °C and an ARIT of 70 °C. The decrease in the evaporation temperature recovers the benefit of the increasing cycle efficiency caused by a recuperator. However, the working fluid mass flow rate is increased due to the higher preheater inlet temperature and the slightly lower evaporation temperature. The optimal evaporation temperature of a RORC using R1336mzz(Z) is 1.1–1.8 °C lower than that of an ORC, but the mass flow rate is 4–5.3% greater for a BIT less than 115 °C and an ARIT of 70 °C. The optimal evaporation temperature of R1233zd(E) is only decreased by 0.2–0.6 °C and the mass flow rate is increased by 0.5–1.6% due to the lower temperature rise in the recuperator, compared to an ORC. The optimal evaporation temperatures for RORCs using R1224yd(Z), R1233zd(E) and R1336mzz(Z) increase by 1.3–2 °C for every 5 °C increase of the BIT, and those using R601a and R601 increase by 1–1.3 °C when the BIT is less than 115 °C and the ARIT is 70 °C, as shown in Figure 4(b2).

The optimal evaporation temperatures for RORCs increase by 4.5–4.7 °C for every 5 °C increase of the BIT as the ARIT increases from 70 °C to 75 °C for the BITs less than 115 °C, as shown in Figure 4(b3); then, the increase in the optimal evaporation temperature decreases as the BIT increases. As the ARIT increases from 70 °C to 75 °C, the optimal evaporation temperatures of R1233zd(E) and R1336mzz(Z) do not change for a BIT higher than 135 °C, while those of R601a and R601 do not change for a BIT higher than almost 130 °C, as shown in Figure 4(b3). Thus, the corresponding reinjection temperatures are higher than 75 °C, as shown in Figure 5(b3). The use of a recuperator reduces the optimal evaporation temperature and the decrease in the evaporation temperature increases as the BIT increases with an ARIT of 75 °C. The decrease in the optimal evaporation temperature for RORC using R1233zd(E) increases from 0.4 °C to 1.6 °C as the BIT increases from 100 °C to 135 °C. The optimal evaporation temperature of a RORC with R1336mzz(Z) is 1.1 °C lower than that of an ORC for a BIT of 100 °C, while 3.9 °C lower for a BIT of 135 °C.

3.2. Net Power Output

Figure 6 shows the maximum net power output for various BITs and ARITs. The maximum turbine power is generated by R1224yd(Z), followed by R1336mzz(Z) and R1233zd€ for a given heat source. The excess of the turbine power produced by R1224yd(Z) over the other selected fluids increases with increasing BIT. The turbine power output with R1224yd(Z) is 2.4% (13 kW) greater than that with R601 for a BIT of 100 °C and is 6.0% (112.8 kW) greater for a BIT of 150 °C with an ARIT of 65 °C. However, the mass flow

rate for R1224yd(Z) is the highest due to the lowest latent heat among the five working fluids. The mass flow rate of R1224yd(Z) is 131.1–138.5% higher than that of R601. The difference between the evaporation and condensation pressures of R1224yd(Z) is also higher than the other four selected fluids at the optimal conditions. The pressure rise in the working fluid pump with R1224yd(Z) is about twice that with R601. Therefore, the working fluid pump power consumption with R1224yd(Z) is greater than the other four working fluids. For instance, the fluid pump with R1224yd(Z) consumes 112.6–124.7% more power than that with R601. Furthermore, the cooling water circulating pump with R1224yd(Z) also consumes 0.6–6.2% more power than the other fluids. The parasitic power consumed by the pumps in an ORC accounts for 10–16.9% of the turbine power output, which decreases as the BIT increases for an ARIT of 65 °C. The total power consumed by the pumps is lower for a working fluid with a higher critical temperature for a given heat source. The net power output of an ORC with R1336mzz(Z) is the highest for a BIT less than 140 °C which is 0.03–0.6% higher than that with R1224yd(Z) due to the smaller parasitic power consumption. The net power output with R1224yd(Z) is 0.3% greater than that with R1336mzz(Z) and 3.6% greater than that with R601 for a BIT of 150 °C and an ARIT of 65 °C, as shown in Figure 6(a1).

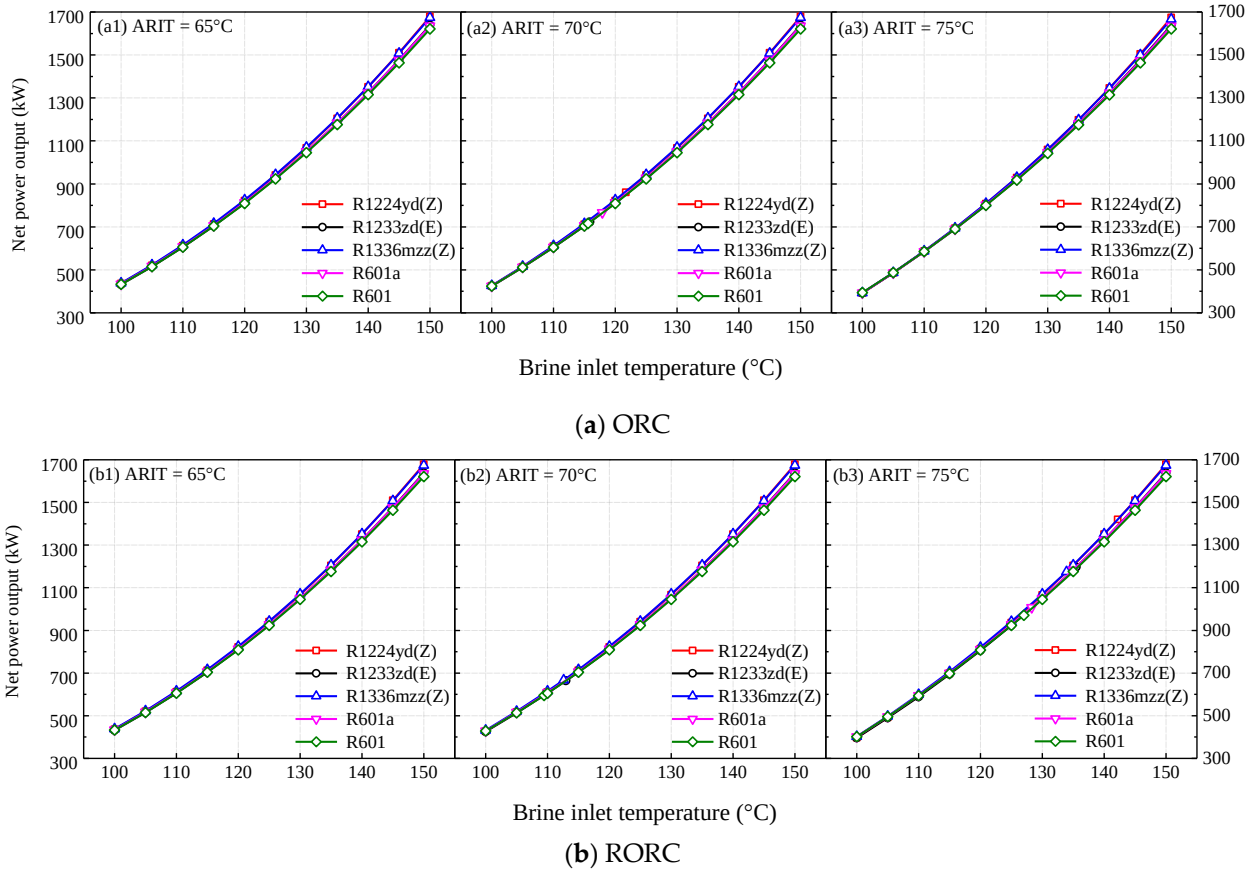

(**a**) ORC

(**b**) RORC

Figure 6. Net power outputs for (**a**) ORCs and (**b**) RORCs at the optimal conditions for various BITs and ARITs.

The working fluid mass flow rate decreases as the ARIT increases since the heat input of the geothermal brine decreases and the evaporation temperature (pressure) increases for a lower BIT. The thermodynamic characteristics of an ORC are greatly affected by the increase in the ARIT for a lower BIT. As the ARIT increases from 65 °C to 70 °C, the cycle thermal efficiency with R601 increases by 9.3% and with R1336mzz(Z) by 10.8%. This is because the evaporation temperature increases, resulting in a lower circulating pump power consumption for a BIT of 100 °C. However, the mass flow rates of the working

fluids decrease by 12.9–15.4% resulting in 3.4–4.4% less turbine power output. The power consumed by the working fluid pump increases by 2.3–2.9% due to the higher pressure rise caused by the increase in the evaporation pressure. The ORC net power outputs for a BIT of 100 °C decrease by 1.9–2.7% (8.1–11.9 kW) as the ARIT increases from 65 °C to 70 °C, as shown in Figure 6a. However, the net power output is not affected for a BIT higher than almost 120 °C. The net power outputs of the five working fluids are very close for BITs less than 120 °C. The net power generated by R1224yd(Z) or R1336mzz(Z) is 1.8–3.6% greater than that by R601 for BITs higher than 120 °C with an ARIT of 70 °C.

As the ARIT further increases from 70 °C to 75 °C, the mass flow rates of the selected fluids decrease by 9.4–18.1% caused by the large decrease in the heat input for BITs less than 120 °C, but the cycle efficiencies increase relatively by 6.8–9.6% with increasing evaporation temperature. The power consumed by the working fluid pump decreases by 2.2–2.9% for a BIT of 100 °C. The turbine power outputs decrease by 8.6–9.2% for a BIT of 100 °C and by 1.9–2.9% for a BIT of 120 °C as the ARIT increases from 70 °C to 75 °C. The net power generated by R1336mzz(Z) at an ARIT of 75 °C is 8% (34.2 kW) lower than that at an ARIT of 70 °C for a BIT of 100 °C and 2% (16.8 kW) lower for a BIT of 120 °C. When the ARIT is 75 °C, the net power output using R1224yd(Z) is 1.2% (10.9 kW) higher than that using R601 for a BIT of 125 °C and is 3.2% (52.6 kW) higher for a BIT of 150 °C, as shown in Figure 6(a3).

For a given heat source, as shown in Figure 6, the net power generated by the RORC is equal to the net power by the ORC because of the same optimal evaporation temperature, as shown in Figure 4 when the ARIT is 65 °C. The decrease in the optimal evaporation temperature of R1336mzz(Z) is greater than the other four fluids as seen in Figure 4(b2) due to the greater temperature rise in the recuperator. Thus, the mass flow rate of the RORC with R1336mzz(Z) is 1.7–5.3% greater than that of an ORC for a BIT less than 120 °C and an ARIT of 70 °C. Thus, the turbine power output of the RORC with R1336mzz(Z) is boosted by 0.2–1.6% (1.9–8.4 kW) considering the decrease in the expansion ratio, compared to an ORC. The power consumed by the working fluid pump in a RORC is lower than that in an ORC since the pressure rise in the pump is reduced, but the power consumed by the circulating pump is greater because the cooling water flow rate is increased for a lower BIT. Therefore, the RORC using R1336mzz(Z) generates 1.2% more net power than the ORC for a BIT of 100 °C and an ARIT of 70 °C. The increase in the net power by the RORC over the ORC decreases as the BIT increases. When the BIT is higher than 120 °C, the RORC and the ORC produce the same net power for an ARIT of 70 °C. When the ARIT is 75 °C, the optimal evaporation temperature for a RORC with R1336mzz(Z) decreases by 1.1 °C for a BIT of 100 °C, 3.9 °C for a BIT of 135 °C and 3.6 °C for a BIT of 150 °C, respectively, compared to that for an ORC. The mass flow rate of R1336mzz(Z) increases by 5.4–8.1% for a RORC but the expansion ratio decreases by 3–9.7%. Therefore, the turbine with R1336mzz(Z) in a RORC outputs 0.8–2.9% more power than that in an ORC. The fluid pump in a RORC consumes less power than that in an ORC due to the lower pressure rise, but the circulating pump consumes more power due to the higher cooling water flow rate. The net power produced by a RORC using R1336mzz(Z) is 2.6% greater than that by an ORC for a BIT of 100 °C and an ARIT of 75 °C, while only 1% greater for a BIT of 130 °C. The RORC with R1233zd(E) generates up to 0.8% more power than an ORC for an ARIT of 75 °C. The excess of the net power generated by a RORC with R1336mzz(Z) over that with R1233zd(E) increases from 6.6 kW to 35.9 kW as the BIT increases from 100 °C to 150 °C with an ARIT of 75 °C. The RORC with R1336mzz(Z) produces 0.2% (1 kW) more net power than that with R601 for a BIT of 100 °C, while 3.3% (53.2 kW) more net power for a BIT of 150 °C and an ARIT of 75 °C.

3.3. Exergy Analyses

3.3.1. Geothermal Exergy Utilization Efficiency

The geothermal exergy utilization efficiency is employed to evaluate the geothermal exergy utilized by the cycle with the different working fluids, which is related to the

BITs and the reinjection temperatures. Figure 7 shows the geothermal exergy utilization efficiencies for ORCs and RORCs at the optimal conditions for various BITs and ARITs. The geothermal exergy utilization efficiency increases with increasing BIT. The ORC with R1336mzz(Z) has the highest geothermal exergy utilization efficiency among the five fluids, as shown in Figure 7(a1), which ranges from 60% to 78.9%, due to the lowest actual reinjection temperature for an ARIT of 65 °C. As the ARIT increases to 70 °C, the geothermal exergy utilization efficiency decreases for a BIT less than 120 °C. As the ARIT increases to 75 °C, the ORCs with the fluids have the same geothermal exergy utilization efficiencies for a given BIT, as shown in Figure 7(a3).

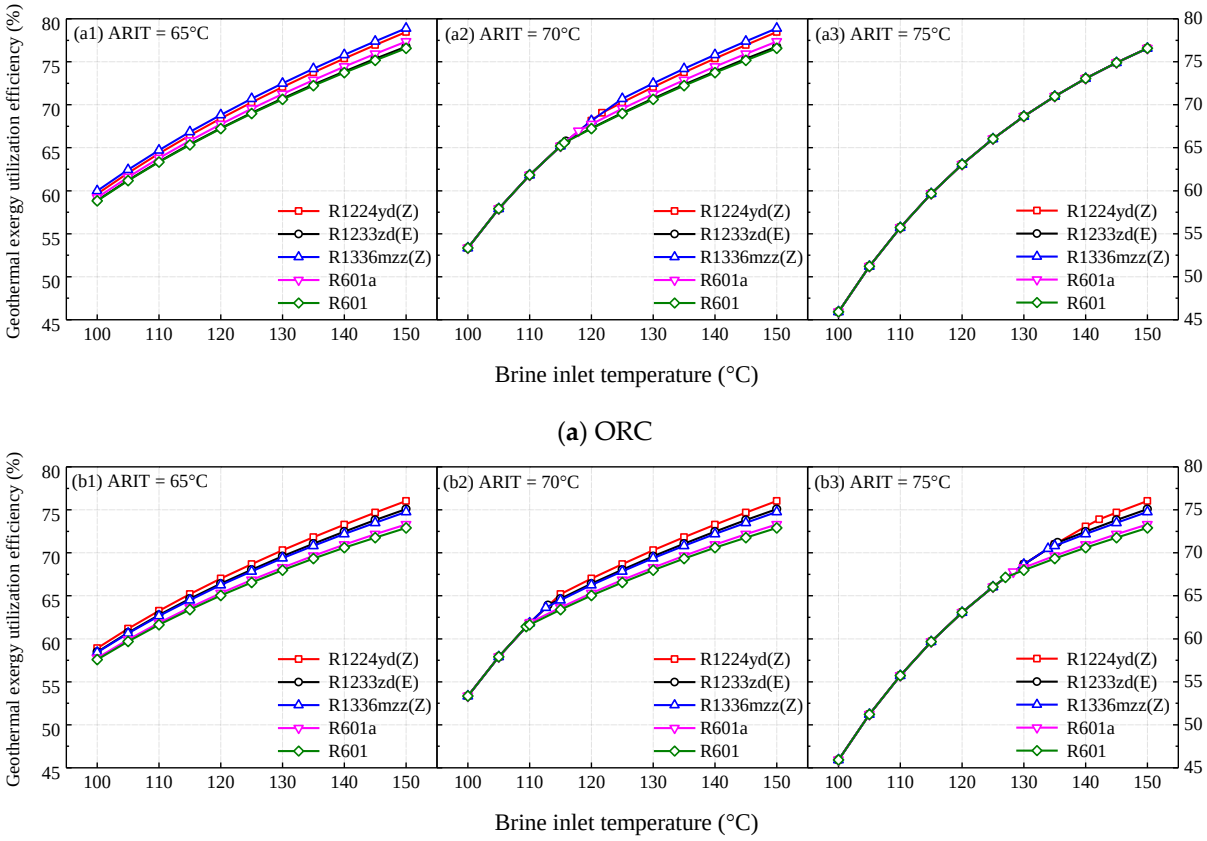

(**a**) ORC

(**b**) RORC

Figure 7. Geothermal exergy utilization efficiencies for (**a**) ORCs and (**b**) RORCs at the optimal conditions for various BITs and ARITs.

The recuperator increases the reinjection temperature as seen in Figure 5(b1), which results in a decrease in the geothermal heat utilization efficiency. The geothermal heat utilization efficiency of a RORC using R1224yd(Z) is the highest among the five fluids, as shown in Figure 7(b1), which increases from 58.9% to 76% for an ARIT of 65 °C, because the reinjection temperature is the lowest, caused by the lower temperature rise in the recuperator. Compared to the ORC, the geothermal heat utilization efficiency with R1233zd(E) is decreased by 0.7–2.2% for the RORC while that with R1336mzz(Z) is decreased by 2.6–5.3% for an ARIT of 65 °C. As the ARIT increases from 65 °C to 70 °C, the geothermal exergy utilization efficiency of a RORC using R1224yd(Z) is decreased by 9.4% for a BIT of 100 °C. However, the geothermal exergy utilization efficiencies of RORCs decrease by 14% for a BIT of 100 °C and by 9.9% for a BIT of 110 °C as the ARIT increases from 70 °C to 75 °C. The geothermal exergy utilization efficiency of a RORC almost does not change for a BIT higher than 130 °C and an ARIT of 75 °C.

3.3.2. Geothermal Heating Exergy Efficiency

The geothermal heating exergy efficiency is used here to evaluate the exergy effectiveness of the heat transfer between the geothermal brine and the working fluid in the preheater and the evaporator. A higher geothermal heating efficiency means fewer irreversible losses during the working fluid heat absorbing process. The geothermal heating exergy efficiency increases with increasing evaporation temperature because the average temperature difference between the brine and the working fluid decreases for a fixed evaporator pinch point temperature difference. However, the geothermal exergy utilization efficiency decreases greatly at a higher evaporation temperature, as seen in Figure 7, because the reinjection temperature correspondingly increases, particularly for a lower BIT.

Figure 8 shows the geothermal heating exergy efficiencies for (a) ORC and (b) RORC at the optimal conditions for various BITs and ARITs. As the ARIT increases, the evaporation temperature should increase for a better match of the temperature profiles of the working fluid and the geothermal brine for a lower BIT as seen in Figure 4. Therefore, the exergy losses during the preheating and evaporating decrease while the geothermal heating exergy efficiency increases. As the ARIT increases to 70 °C from 65 °C, the geothermal heating exergy efficiencies of ORCs are increased by 4–4.5% for a BIT of 100 °C, as shown in Figure 8a. Thus, the exergy losses in the preheater and evaporator are decreased by 16.7–19%. The geothermal heating exergy efficiency of an ORC with R1336mzz(Z) is increased by 2.1% and that with R1233zd(E) is increased by 1.2% for a BIT of 110 °C. The geothermal heating exergy efficiency does not change as the ARIT increases from 65 °C to 70 °C due to the same optimal evaporation temperature for a BIT higher than 125 °C. As the ARIT increases from 70 °C to 75 °C, the optimal evaporation temperatures of the selected fluids are increased by 4.4–4.8 °C for BITs lower than 120 °C; thus, the geothermal heating exergy efficiencies are increased by 3–3.9% for an ORC, as shown in Figure 8a. When the BIT is higher than 120 °C, the increase in the geothermal heating exergy efficiency decreases as the BIT increases. The geothermal heating exergy efficiency with R1336mzz(Z) is still increased by 1.6% and that with R1224yd(Z) is increased by 1.3% as the ARIT increases to 75 °C from 70 °C for a BIT of 150 °C due to the higher evaporation temperature.

The RORC has the same optimal evaporation temperature as the ORC for an ARIT of 65 °C, as seen in Figure 4(b1), but the preheater inlet temperature is greater resulting in a better match between the temperatures of the working fluid and the geothermal brine. Therefore, the geothermal heating exergy efficiency of a RORC is greater than that of an ORC, as shown in Figure 8(a1,b1). The increase in the geothermal heating exergy efficiency of a RORC over an ORC increases as the BIT increases due to the greater temperature rise in the recuperator for an ARIT of 65 °C. For instance, the geothermal heating exergy efficiencies of RORCs with R1336mzz(Z), R601a and R601 are 1.2–1.4% greater than those of ORCs for a BIT of 100 °C and 2.7–2.9% greater for a BIT of 150 °C. When the ARIT is 70 °C, the increase in the geothermal heating exergy efficiency of a RORC over an ORC first decreases and then increases with increasing BIT because of the lower evaporation temperature for a BIT less than 115 °C. For instance, the geothermal heating exergy efficiency of a RORC with R1336mzz(Z) is 0.9% greater for a BIT of 100 °C, 0.4% greater for a BIT of 115 °C and 2.8% greater for a BIT of 150 °C than that of an ORC. The optimal evaporation temperature of a RORC with R1336mzz(Z) is decreased by 1.1 °C for a BIT of 100 °C, by 3.9 °C for a BIT of 135 °C and 3.7 °C for a BIT of 150 °C with an ARIT of 75 °C. Thus, the increase in the geothermal heating exergy efficiency of a RORC with R1336mzz(Z) over an ORC decreases from 1.7% to 0.4% as the BIT increases from 100 °C to 135 °C, and then increases to 1.3% as the BIT further increases to 150 °C, as shown in Figure 8. The geothermal heating exergy efficiency of a RORC with R1233zd(E) is the lowest for a BIT higher than 130 °C due to the lowest preheater inlet temperature.

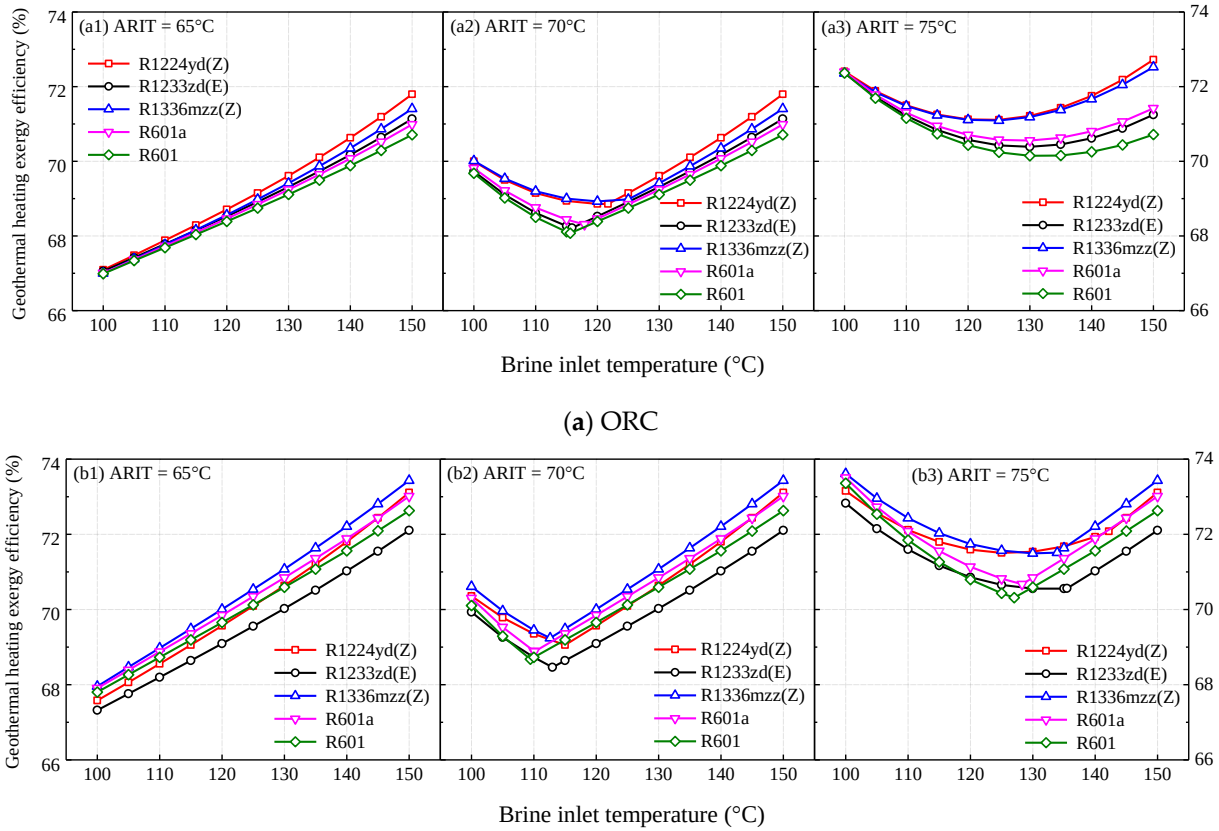

Figure 8. Geothermal heating exergy efficiencies for (**a**) ORC and (**b**) RORC at the optimal conditions for various ARITs and BITs.

3.3.3. Cycle Internal Exergy Efficiency

The cycle internal exergy efficiency is defined as the ratio of the net power to the net exergy input of the cycle. The internal exergy efficiency reflects the total exergy losses in the turbine, generator, working fluid pump, recuperator, condenser and cooling system. Figure 9 shows the cycle internal exergy efficiencies at the optimal conditions for ORCs and RORCs for various BITs and ARITs. The cycle internal exergy efficiency proportional follows the changes of the BIT, as shown in Figure 9. The cycle internal irreversibility losses mainly occur in the condenser and the cooling system. For instance, the exergy losses in the condenser and the cooling system account for 66.7–72.9% of the total cycle internal exergy losses for a BIT of 100 °C and 58–63.5% for a BIT of 150 °C. The cycle internal exergy efficiencies for ORCs with the selected working fluids are very close for a BIT less than 120 °C. R1233zd(E) has a slightly higher cycle internal exergy efficiency when the BIT is higher than 130 °C, as shown in Figure 9(a1). The exergy destruction rate of the condenser and the cooling system is reduced in a RORC, since part of the turbine exhaust heat is recovered for fluid preheating. Thus, the cycle internal exergy efficiency of a RORC is greater than that of an ORC, especially for a higher BIT, as shown in Figure 9b. The cycle internal exergy efficiencies for RORCs using R1336mzz(Z), R601a and R601 can be relatively improved by 1.3–2.6% for a BIT higher than 120 °C and an ARIT of 65 °C compared to an ORC. As the ARIT increases from 65 °C to 70 °C, the cycle internal exergy efficiency for an ORC is increased by 4–4.6% because of the increase in the evaporation temperature and the decrease in the exergy destruction rate of the condenser and the cooling system for a BIT of 100 °C, while it does not change for a BIT higher than 120 °C. As the ARIT increases from 70 °C to 75 °C, the cycle internal exergy efficiency of an ORC is increased relatively by 1.1–3.8% for a BIT less than 130 °C. The cycle internal exergy efficiencies for RORCs with R1336mzz(Z), R601a and R601 are 1–2.6% greater than those of ORCs for the considered

allowed reinjection temperatures. The increase in the cycle internal exergy efficiency of RORC over that of ORC increases with increasing BIT.

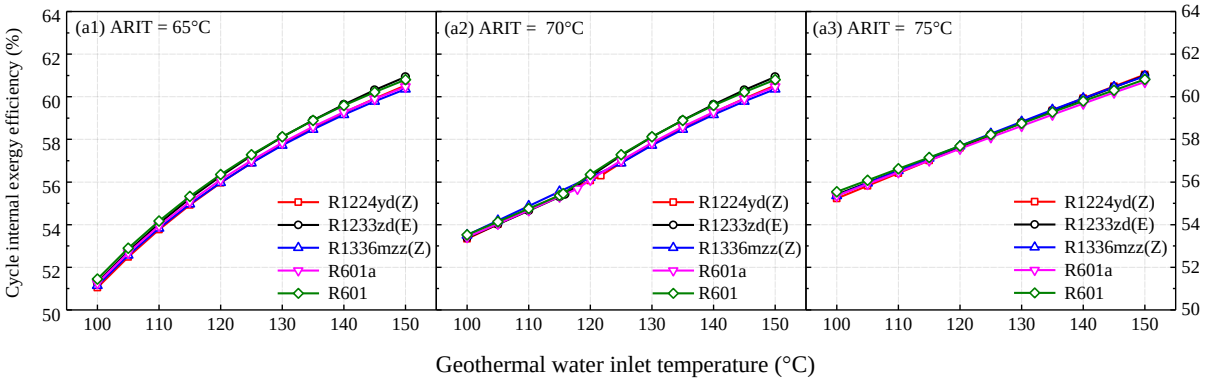

(**a**) BORC

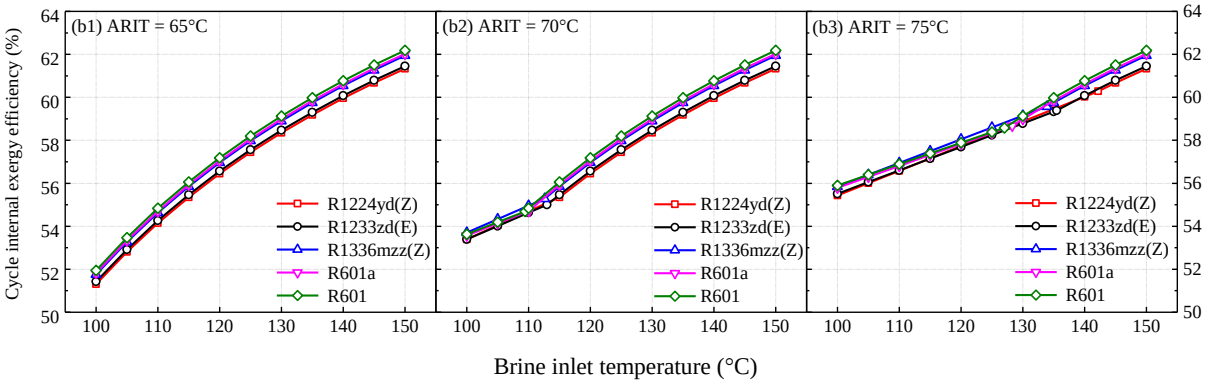

(**b**) RORC

Figure 9. Cycle internal exergy efficiencies for (**a**) ORCs and (**b**) RORCs at the optimal conditions for various BITs and ARITs.

3.3.4. Plant Exergy Efficiency

Figure 10 shows the plant exergy efficiencies of ORCs and RORCs for the optimal conditions. The plant exergy efficiency continues to increase with increasing BIT. The plant exergy efficiencies of the ORCs with the five working fluids are very close for BITs lower than 120 °C. The difference between the ORC plant exergy efficiencies with the five fluids for a given BIT is smaller for a higher ARIT. The plant exergy efficiency of an ORC with R1336mzz(Z) is 1.3% relatively higher than that with R601 for a BIT of 100 °C, while it is 3.3% relatively higher for a BIT of 150 °C when the ARIT is 65 °C. As the ARIT increases from 65 °C to 70 °C, the plant exergy efficiency as well as the net power output of ORC with R1336mzz(Z) decreases by 2.7% for a BIT of 100 °C but does not change for BITs higher than 120 °C. As the ARIT increases from 70 °C to 75 °C, the plant exergy efficiencies of ORCs and RORCs are decreased by less than 1% for BITs higher than 120 °C but are decreased by 7.3–8.0% for a BIT of 100 °C due to the larger decrease in the net power output. The plant exergy efficiency of an ORC with R1336mzz(Z) is 20.0% for an ARIT of 65 °C and a BIT of 100 °C, while it reduces to 18.4% for an ARIT of 75 °C. Furthermore, the decrease in the plant exergy efficiency caused by the increase in the ARIT for ORC with R1336mzz(Z) is the highest among the five working fluids for a lower BIT. The plant exergy efficiency of a RORC is obviously greater than an ORC for a lower BIT and a higher ARIT. The plant exergy efficiency of a RORC with R1336mzz(Z) can be increased by up to 2.6% for an ARIT of 75 °C, which means the highest increase among the selected fluids. Therefore, the decrease in the plant exergy efficiency caused by the increase in the ARIT for RORC with R1336mzz(Z) is smaller than that for ORC. For RORCs, the decrease in the plant exergy

efficiency due to the increase in the ARIT with R1224yd(Z) is slightly higher than that with the other selected fluids.

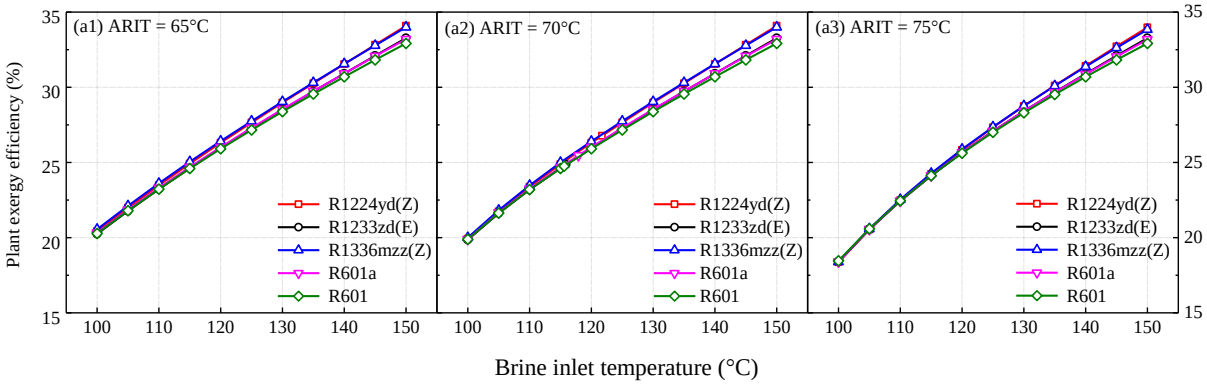

(**a**) ORC

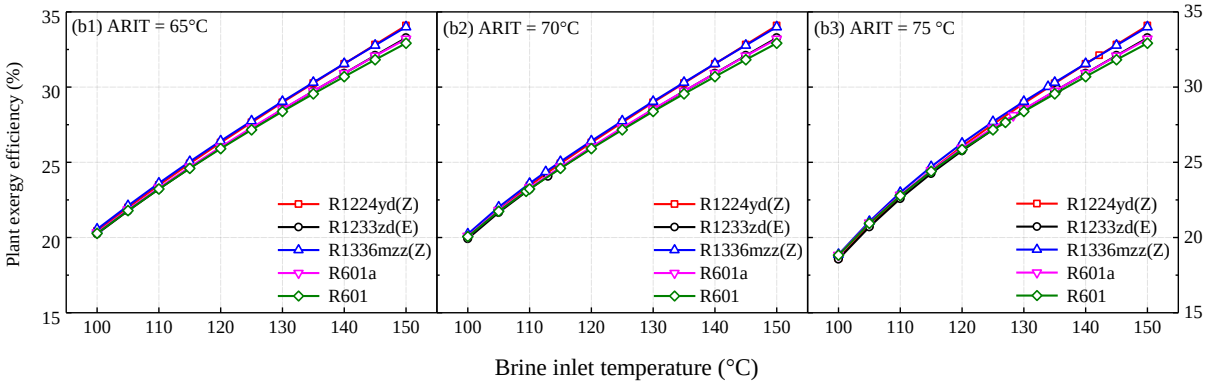

(**b**) RORC

Figure 10. Plant exergy efficiencies for (**a**) ORCs and (**b**) RORCs at the optimal conditions for various ARITs and BITs.

4. Conclusions

The thermodynamic characteristics of ORCs and RORCs were studied with the consideration of the influences of the allowed reinjection temperature (ARIT). The evaporation temperatures of R1224yd(Z), R1233zd(E), R1336mzz(Z), R601a and R601 were optimized for the maximal net power output for brine inlet temperatures (BITs) from 100 °C to 150 °C and allowed reinjection temperatures (ARITs) from 65 °C to 75 °C. The results show that:

1. The optimal evaporation temperature of an ORC with R1224yd(Z) is higher than that with R1336mzz(Z), R1233zd(E), R601a and R601. As the allowed reinjection temperature (ARIT) increases, the evaporation temperature should increase for a better temperature match with the geothermal brine. The optimal evaporation temperatures for RORCs are lower than those for ORCs for a brine inlet temperature (BIT) less than 120 °C and an ARIT higher than 70 °C.
2. The maximum turbine work power of an ORC is generated by R1224yd(Z), followed by R1336mzz(Z) and R1233zd(E) for the same geothermal source and the reinjection temperature limit. However, the pumps in an ORC with 1224yd(Z) consumed more parasitic power than the other four fluids due to the higher mass flow rate. An ORC with R1336mzz(Z) generates 1–3% more net power than that with R1233zd(E), R601a and R601 for BITs above 120 °C due to the higher geothermal exergy utilization efficiency and the lower exergy losses in the evaporator and the preheater.
3. Compared to ORC, RORC has a higher preheater inlet temperature, which results in a higher geothermal heating exergy efficiency for a BIT lower than 120 °C and generates about 1% more net power. The RORC using R1336mzz(Z) produces 2.6% more net

power than an ORC for a brine inlet temperature of 100 °C and an allowed reinjection temperature of 75 °C, while only 1% more net power for a brine inlet temperature of 130 °C.

4. As the allowed reinjection temperature increases, the geothermal exergy utilization efficiency and the exergy loss during the working fluid heat absorption decrease, especially for lower BITs. As the allowed reinjection temperature increases from 70 °C to 75 °C, the plant exergy efficiencies of ORCs decrease by less than 1% for BITs above 120 °C and decrease by 6–8% for a BIT of 100 °C.

Author Contributions: Conceptualization, Y.Z. and Q.L.; methodology, Y.Z., C.G. and J.S.; software, C.G. and J.S.; validation, C.L. and C.W.; formal analysis, Y.Z., C.L. and Q.L.; investigation, Y.Z., C.G. and J.S.; writing—original draft preparation, Y.Z., J.S. and Q.L.; writing—review and editing, Y.Z., C.W. and Q.L.; visualization, Y.Z., C.G. and C.W.; resources, C.L. and Q.L.; supervision, Q.L. and J.Z.; project administration, C.W. and Q.L.; funding acquisition, Q.L. All authors have read and agreed to the published version of the manuscript.

Funding: This research was funded by the National Natural Science Foundation of China, grant number 51736005 and 51506223.

Institutional Review Board Statement: Not applicable.

Informed Consent Statement: Not applicable.

Data Availability Statement: Not applicable.

Conflicts of Interest: The authors declare no conflict of interest.

Nomenclature

$\dot{E}$	exergy (kW)
g	gravitational acceleration ($m \cdot s^{-2}$)
h	specific enthalpy ($kJ \cdot kg^{-1}$)
H	pump head (m)
$\dot{I}$	exergy destruction (kW)
$\dot{m}$	mass flow rate ($kg \cdot s^{-1}$)
p	pressure (MPa)
$\dot{Q}$	heat flow (kW)
s	specific entropy ($kJ \cdot kg^{-1} \cdot K^{-1}$)
t	temperature (°C)
T	temperature (K)
$\dot{W}$	power (kW)
Abbreviations	
ARIT	allowed reinjection temperature
BIT	brine inlet temperature
CP	cooling water circulating pump
CON	condenser
CP	cooling water circulating pump
CW	cooling water
E	evaporator
FP	working fluid feed pump
GEN	generator
ORC	organic Rankine cycle
FP	working fluid feed pump
g	generator
GH	geothermal heating
GU	geothermal exergy utilization
in	inlet
m	mechanical
net	net

O	organic working fluid
plant	geothermal power plant
s	isentropic
T	turbine
R1224yd(Z)	cis-1-chloro-2,3,3,3-tetrafluoropropene
R1233zd(E)	trans-1-chloro-3,3,3-trifluoropropene
R1336mzz(Z)	trans-1,1,1,4,4,4-Hexafluoro-2-butene
R601	pentane
R601a	isopentane
Greek letters	
η	efficiency
Superscripts	
ex	exergy

References

1. Wang, Y.Z.; Li, C.J.; Zhao, J.; Wu, B.Y.; Du, Y.P.; Zhang, J.; Zhu, Y.L. The above-ground strategies to approach the goal of geothermal power generation in China: State of art and future researches. *Renew. Sustain. Energy Rev.* **2021**, *138*, 110557. [CrossRef]
2. Franco, A.; Vaccaro, M. Numerical simulation of geothermal reservoirs for the sustainable design of energy plants: A review. *Renew. Sustain. Energy Rev.* **2014**, *30*, 987–1002. [CrossRef]
3. Top 10 Geothermal Countries Power Generation. Available online: https://www.thinkgeoenergy.com/thinkgeoenergys-top-10-geothermal-countries-2021-installed-power-generation-capacity-mwe/ (accessed on 18 June 2022).
4. Bertani, R. Geothermal power generation in the world 2010–2014 update report. *Geothermics* **2016**, *60*, 31–43. [CrossRef]
5. Zhu, J.L.; Hu, K.Y.; Zhang, W.; Lu, X.L. A study on generating a map for selection of optimum power generation cycles used for Enhanced Geothermal Systems. *Energy* **2017**, *133*, 502–512. [CrossRef]
6. Bett, A.K.; Jalilinasrabady, S. Optimization of ORC Power Plants for Geothermal Application in Kenya by Combining Exergy and Pinch Point Analysis. *Energies* **2021**, *14*, 6579. [CrossRef]
7. Yang, X.F.; Xu, J.L.; Miao, Z.; Zou, J.H.; Qi, F.L. The definition of non-dimensional integration temperature difference and its effect on organic Rankine cycle. *Appl. Energy* **2016**, *167*, 17–33. [CrossRef]
8. Lecompte, S.; Huisseune, H.; Broek, M.V.D.; Vanslambrouck, B.; Paepe, M.D. Review of organic Rankine cycle (ORC) architectures for waste heat recovery. *Renew. Sustain. Energy Rev.* **2015**, *47*, 448–461. [CrossRef]
9. Zhai, H.X.; An, Q.S.; Shi, L.; Lemort, V.; Quoilin, S. Categorization and analysis of heat sources for organic Rankine cycle systems. *Renew. Sustain. Energy Rev.* **2016**, *64*, 790–805. [CrossRef]
10. Astolfi, M.; Romano, M.C.; Bombarda, P.; Macchi, E. Binary ORC (Organic Rankine Cycles) power plants for the exploitation of medium-low temperature geothermal sources—Part A: Thermodynamic optimization. *Energy* **2014**, *66*, 423–434. [CrossRef]
11. Manente, G.; Lazzaretto, A.; Bonamico, E. Design guidelines for the choice between single and dual pressure layouts in organic Rankine cycle (ORC). systems. *Energy* **2017**, *123*, 413–431. [CrossRef]
12. Baccioli, A.; Antonelli, M.; Desideri, U. Technical and economic analysis of organic flash regenerative cycles (OFRCs) for low temperature waste heat recovery. *Appl. Energy* **2017**, *199*, 69–87. [CrossRef]
13. Meng, N.; Li, T.L.; Gao, X.; Liu, Q.H.; Li, X.L.; Gao, H.Y. Thermodynamic and techno-economic performance comparison of two-stage series organic Rankine cycle and organic Rankine flash cycle for geothermal power generation from hot dry rock. *Appl. Therm. Eng.* **2022**, *200*, 117715. [CrossRef]
14. Franco, A.; Villani, M. Optimal design of binary cycle power plants for water-dominated, medium-temperature geothermal fields. *Geothermics* **2009**, *38*, 379–391. [CrossRef]
15. Quoilin, S.; Broek, M.V.D.; Declaye, S.; Dewallef, P.; Lemort, V. Techno-economic survey of organic Rankine cycle (ORC) systems. *Renew. Sustain. Energy Rev.* **2013**, *22*, 168–186. [CrossRef]
16. Hu, S.; Yang, Z.; Li, J.; Duan, Y. A Review of Multi-Objective Optimization in Organic Rankine Cycle (ORC) System Design. *Energies* **2021**, *14*, 6492. [CrossRef]
17. Basaran, A.; Ozgerer, L. Investigation of the effect of different refrigerants on performances of binary geothermal power plants. *Energy Convers. Manag.* **2013**, *76*, 483–498. [CrossRef]
18. Méndez-Cruz, L.E.; Gutiérrez-Limón, M.Á.; Lugo-Méndez, H.; Lugo-Leyte, R.; Lopez-Arenas, T.; Sales-Cruz, M. Comparative Thermodynamic Analysis of the Performance of an Organic Rankine Cycle Using Different Working Fluids. *Energies* **2022**, *15*, 2588. [CrossRef]
19. Li, J.; Ge, Z.; Duan, Y.Y.; Yang, Z.; Liu, Q. Parametric optimization and thermodynamic performance comparison of single-pressure and dual-pressure evaporation organic Rankine cycles. *Appl. Energy* **2018**, *217*, 409–421. [CrossRef]
20. Li, J.; Ge, Z.; Liu, Q.; Duan, Y.Y.; Yang, Z. Thermo-economic performance analyses and comparison of two turbine layouts for organic Rankine cycles with dual-pressure evaporation. *Energy Convers. Manag.* **2018**, *164*, 603–614. [CrossRef]
21. Luo, X.L.; Huang, R.L.; Yang, Z.; Chen, J.Y.; Chen, Y. Performance investigation of a novel zeotropic organic Rankine cycle coupling liquid separation condensation and multi-pressure evaporation. *Energy Convers. Manag.* **2018**, *161*, 112–127. [CrossRef]

22. Karimi, S.; Mansouri, S. A comparative profitability study of geothermal electricity production in developed and developing countries: Exergoeconomic analysis and optimization of different ORC configurations. *Renew. Energy* **2018**, *115*, 600–619. [CrossRef]
23. Du, Y.; Yang, Y.; Hu, D.S.; Hao, M.T.; Wang, J.F.; Dai, Y.P. Off-design performance comparative analysis between basic and parallel dual-pressure organic Rankine cycles using radial inflow turbines. *Appl. Therm. Eng.* **2018**, *138*, 18–34. [CrossRef]
24. Bina, S.M.; Jalilinasrabady, S.; Fujii, H. Thermo-economic evaluation of various bottoming ORCs for geothermal power plant, determination of optimum cycle for Sabalan power plant exhaust. *Geothermics* **2017**, *70*, 181–191. [CrossRef]
25. Yari, M. Exergetic analysis of various types of geothermal power plants. *Renew. Energy* **2010**, *35*, 112–121. [CrossRef]
26. Spadacini, C.; Xodo, L.G.; Quaia, M. Geothermal energy exploitation with Organic Rankine Cycle technologies. In *Organic Rankine Cycle (ORC) Power Systems*; Macchi, E., Astolfi, M., Eds.; Elsevier: Amsterdam, The Netherlands, 2017; pp. 473–525. [CrossRef]
27. Macchi, E. Theoretical basis of the organic Rankine cycle. In *Organic Rankine Cycle (ORC) Power Systems*; Macchi, E., Astolfi, M., Eds.; Elsevier: Amsterdam, The Netherlands, 2017; pp. 3–24. [CrossRef]
28. Eyerer, S.; Dawo, F.; Kaindl, J.; Wieland, C.; Spliethoff, H. Experimental investigation of modern ORC working fluids R1224yd (Z) and R1233zd (E) as replacements for R245fa. *Appl. Energy* **2019**, *240*, 946–963. [CrossRef]
29. Welzl, M.; Heberle, F.; Weith, T.; Brüggemann, D. Experimental Evaluation of R1336mzz (Z) as Low GWP Replacement for R245fa in a Scroll Expander. In Proceedings of the 5th International Seminar on ORC Power Systems, Athens, Greece, 9–11 September 2019.
30. Dawo, F.; Fleischmann, J.; Kaufmann, F.; Schifflechner, C.; Eyerer, S.; Wieland, C.; Spliethoff, H. R1224yd(Z), R1233zd(E) and R1336mzz(Z) as replacements for R245fa: Experimental performance, interaction with lubricants and environmental impact. *Appl. Energy* **2021**, *288*, 116661. [CrossRef]
31. Longo, G.A.; Mancin, S.; Righetti, G.; Zilio, C.; Brown, J.S. Assessment of the low-GWP refrigerants R600a, R1234ze (Z) and R1233zd (E) for heat pump and organic Rankine cycle applications. *Appl. Therm. Eng.* **2020**, *167*, 114804. [CrossRef]
32. Qiu, K.; Entchev, E. A micro-CHP system with organic Rankine cycle using R1223zd (E) and n-Pentane as working fluids. *Energy* **2022**, *239*, 121826. [CrossRef]
33. Ye, Z.; Yang, J.; Shi, J.; Chen, J.P. Thermo-economic and environmental analysis of various low-GWP refrigerants in Organic Rankine cycle system. *Energy* **2020**, *199*, 117344. [CrossRef]
34. Zhang, C.; Fu, J.; Yuan, P.; Liu, J. Guidelines for Optimal Selection of Subcritical Low-Temperature Geothermal Organic Rankine Cycle ConFigureuration Considering Reinjection Temperature Limits. *Energies* **2018**, *11*, 2878. [CrossRef]
35. Lemmon, E.W.; Bell, I.H.; Huber, M.L.; McLinden, M.O. *NIST Standard Reference Database 23: Reference Fluid Thermodynamic and Transport Properties-Refprop, Version 10.0*; NIST: Gaithersburg, MD, USA, 2018.
36. Kamila, Z.; Kaya, E.; Zarrouk, S.J. Reinjection in geothermal fields: An updated worldwide review 2020. *Geothermics* **2021**, *89*, 101970. [CrossRef]
37. Liu, Q.; Duan, Y.Y.; Yang, Z. Performance analyses of geothermal organic Rankine cycles with selected hydrocarbon working fluids. *Energy* **2013**, *63*, 123–132. [CrossRef]
38. Zhang, X.; Zhang, Y.; Cao, M.; Wang, J.; Wu, Y.; Ma, C. Working Fluid Selection for Organic Rankine Cycle Using Single-Screw Expander. *Energies* **2019**, *12*, 3197. [CrossRef]
39. Sun, J.; Liu, Q.; Duan, Y.Y. Effects of evaporator pinch point temperature difference on thermo-economic performance of geothermal organic Rankine cycle systems. *Geothermics* **2018**, *75*, 249–258. [CrossRef]
40. Zhang, C.; Liu, C.; Xu, X.X.; Li, Q.B.; Wang, S.K.; Chen, X. Effects of superheat and internal heat exchanger on thermo-economic performance of organic Rankine cycle based on fluid type and heat sources. *Energy* **2018**, *159*, 482–495. [CrossRef]